Coulomb effects on strong-field ionization of stretched H_2^+

S. Q. Shen,[1,*] Z. Y. Chen,[1,*] S. Wang,[2] J. Y. Che,[1] and Y. J. Chen[1,†]
[1]*College of Physics and Information Technology, Shaan'xi Normal University, Xi'an 710119, China*
[2]*School of Physics, Hebei Normal University, Shijiazhuang 050024, China*

(Received 11 July 2024; revised 30 August 2024; accepted 3 September 2024; published 13 September 2024)

We numerically and analytically study ionization of H_2^+ with large internuclear distances R in strong elliptically polarized laser fields. Numerical simulations show that the offset angle in the photoelectron momentum distribution (PMD) is larger for cases of large R than for cases of H_2^+ with small R and model atoms with similar ionization potentials. In addition, the PMDs for cases of large R show clear interference patterns which disappear for cases of small R. By developing a strong-field model which includes the contributions of the first excited state and the Coulomb potential, we reproduce the phenomena for large R. Tunneling ionization of H_2^+ with large R involves a complex four-body interaction between the laser, the electron, and the two nuclei. Our model can approximate the four-body interaction as the three-body one and clearly identify the effects of charge resonance and different nuclei on tunneling ionization. Our work suggests a manner for probing complex interactions in strong-field ionization of stretched molecules with high time resolution.

DOI: 10.1103/PhysRevA.110.033106

I. INTRODUCTION

Due to advancements in laser technology, the study of interactions between strong lasers and atoms [1–3], molecules [4,5], and solids [6] has become increasingly popular in strong-field physics. When the intensity of the laser field matches the Coulomb potential of the system, many interesting processes occur, such as high-order harmonic generation [7–11], above-threshold ionization [12–18], and nonsequential double ionization [19–21]. These processes have wide applications in attosecond-resolved ultrafast measurements [22–24]. The first step in these processes is the ionization of electrons through tunneling [25]. Systematic and comprehensive research has been conducted on tunneling ionization of atoms and molecules with small internuclear distances R. For example, in the well-known attoclock experiment [26,27], the tunneling dynamics of atoms has been studied using the offset angle in the photoelectron momentum distribution (PMD) measured in a strong elliptically polarized laser field and the main impact of the long-range Coulomb potential on ionization has been revealed [28–30]. In addition, for molecules with small R such as H_2^+ at the equilibrium separation, it has been shown that the multicenter Coulomb potential also plays an important role in the strong-field tunneling dynamics of the system [31].

By comparison, studies on tunneling ionization of molecules with large R are less common. For H_2^+ with large R, it has been shown that the ground state and the first excited state are nearly degenerate. As a result, besides the ground state, the excited state also plays a nontrivial role in tunneling ionization of the stretched system [32–35]. In this case, it is not clear how the interplay of the excited state and the Coulomb potential affects the dynamics of tunneling ionization. Specifically, the strong-field approximation (SFA) [36], which is often used for studying laser-induced ionization of atoms and molecules, assumes that, except for the ground state, the contributions of other bound states to ionization can be ignored [3,36]. This assumption is applicable for atoms and molecules with small R, for which the energy gap between the ground state and the first excited state of the system is usually far larger than the laser frequency used in experiments [37]. For symmetric molecular ions such as H_2^+ with large R, however, the situation is very different. It has been shown that at large R, a degeneracy between these two lowest states of the H_2^+ system occurs [38], which are well separated from higher excited states of the system. In intense laser fields, these two degenerate states will be strongly coupled together, resulting in the important contribution of the excited state to ionization [33,34,38]. In addition, a great deal of studies have shown that the Coulomb potential plays an important role in the strong-field ionization process, remarkably affecting the photoelectron momentum [26], angular distributions [39], and energy spectra [23]. One can anticipate that the interaction of the excited state and the Coulomb potential will induce complex effects in strong-field ionization. To understand these effects, a theoretical model that considers the influences of both the excited state and the Coulomb potential is needed. In this paper, through numerically solving the time-dependent Schrödinger equation (TDSE) and developing a strong-field model applicable for molecular ions with large R, we study the ionization dynamics of the H_2^+-like model ion with different internuclear distances R but similar ionization potential I_p for various laser parameters.

The TDSE results show two typical phenomena. First, the PMDs of H_2^+ with large R show remarkable interference fringes. This interference phenomenon disappears for cases

*These authors contributed equally to this work.
†Contact author: chenyjhb@gmail.com

of small R. Second, the offset angle θ in the PMD for H_2^+ with large R is larger than that for model atoms and molecules with small R. With the developed model, we show that (i) for molecules with large R, the strong coupling between the ground state and the first excited state of the system plays an important role in the formation of interference patterns in tunneling ionization and (ii) the laser-dressed potential for H_2^+ with large R shows two barriers: one dressed up and another dressed down. The dressed-up potential barrier near one nucleus is significantly influenced by another nucleus, making it narrower. As a result, electrons tend to tunnel through the dressed-up potential barrier with a smaller exit position. This tendency leads to a larger offset angle θ and ionization probability compared to model atoms and molecules with small R. Our results suggest a method for studying tunneling-ionization dynamics of electrons within stretched molecules.

II. NUMERICAL AND ANALYTICAL METHODS

A. Numerical method

We choose the simplest diatomic molecule H_2^+ as the target molecule. In the length gauge, the Hamiltonian of the model H_2^+ system interacting with a strong laser field can be written as

$$H(t) = H_0 + \mathbf{E}(t)\cdot\mathbf{r} \tag{1}$$

(in atomic units of $\hbar = e = m_e = 1$). Here $H_0 = \mathbf{p}^2/2 + V(\mathbf{r})$ is the field-free Hamiltonian. The potential $V(\mathbf{r})$ has the form of $V(\mathbf{r}) = -Z/\sqrt{r_1^2+\xi} - Z/\sqrt{r_2^2+\xi}$, with $r_{1,2}^2 = (x \pm R/2\cos\theta')^2 + (y \pm R/2\sin\theta')^2$ in two-dimensional (2D) cases. The term $\xi = 0.5$ is the smoothing parameter which is used to avoid the Coulomb singularity. Here θ' is the angle between the molecular axis and the major axis of the laser polarization ellipse and we consider the parallel orientation with $\theta' = 0°$. The term Z is the effective charge, which is adjusted so that the model molecules with different internuclear distances R studied here have the same ionization energy $I_p = 1.11$ a.u. Specifically, in our simulations, $Z = 1$ for $R = 2$ a.u., $Z = 1.55$ for $R = 12$ a.u., $Z = 1.57$ for $R = 14$ a.u., $Z = 1.585$ for $R = 16$ a.u., $Z = 1.597$ for $R = 18$ a.u., and $Z = 1.607$ for $R = 20$ a.u.

The strong elliptically polarized laser field used in the paper is expressed as $\mathbf{E}(t) = f(t)[\vec{\mathbf{e}}_x E_x(t) + \vec{\mathbf{e}}_y E_y(t)]$, where $E_x(t) = E_0\sin(\omega t)$ and $E_y(t) = E_1\cos(\omega t)$, with $E_0 = E_L/\sqrt{1+\varepsilon^2}$ and $E_1 = \varepsilon E_L/\sqrt{1+\varepsilon^2}$. Here $\vec{\mathbf{e}}_x$ ($\vec{\mathbf{e}}_y$) is the unit vector along the x (y) axis, E_L is the maximal laser amplitude corresponding to the peak intensity I, $\varepsilon = 0.87$ is the ellipticity, ω is the laser frequency, and $f(t)$ is the envelope function. In numerical calculations, we use trapezoid-shaped laser pulses with a total duration of 15 optical cycles and linear ramps of three optical cycles. The spectral method [40] is used to solve the time-dependent Schrödinger equation with a time step of $\triangle t = 0.05$ a.u., a grid size of $L_x \times L_y = 409.6\times409.6$ a.u., and space steps of $\triangle x = \triangle y = 0.4$ a.u.

In order to avoid the reflection of the electron wave packet from the boundary and obtain the momentum-space wave function, the coordinate space is split into the inner and outer regions with $\Psi(\mathbf{r},t) = \Psi_{\text{in}}(\mathbf{r},t) + \Psi_{\text{out}}(\mathbf{r},t)$, by multiplication using a mask function, which has the form

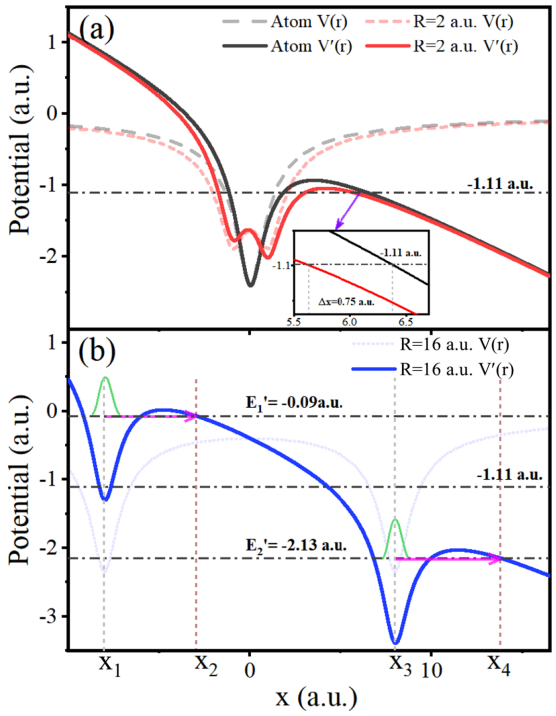

FIG. 1. Potential function curves obtained at different laser and molecular parameters. (a) Sketch of the laser-dressed potential $V'(\mathbf{r}) = V(\mathbf{r}) - E_0 x$ (solid curves) and laser-free potential $V(\mathbf{r})$ (dash-dotted line) for 2D H_2^+ with $R = 2$ a.u. (red curves) and the model atom (black curves) at $y = 0$. The horizontal line indicates the energy of $-I_p = -1.11$ a.u. The inset shows a close-up of the results for the difference in exit position between the molecule and the atom. (b) Sketch of the laser-dressed potential $V'(\mathbf{r}) = V(\mathbf{r}) - E_0 x$ (solid curves) and laser-free potential $V(\mathbf{r})$ (dash-dotted lines) for 2D H_2^+ with $R = 16$ a.u. at $y = 0$. Two horizontal lines represent the energy $E_1' \approx -[I_p - E_0(R/2)] = -0.09$ a.u. and the energy $E_2' \approx -[I_p + E_0(R/2)] = -2.13$ a.u., respectively. The coordinate x_2 (x_4) corresponds to the exit position of electrons tunneling out of the dressed-up (down) potential barrier neighboring the left (right) nucleus. The coordinates x_1 and x_3 represent the positions of the left and right nuclei of the molecule. The horizontal pink arrows indicate the direction of tunneling and $r_0'' = |x_2 - x_1|$ ($r_0'' = |x_4 - x_3|$) represents the absolute value of the exit position relative to the position of the left (right) nucleus. The laser amplitude E_0 used here is $E_0 = 0.13$ a.u.

$F(\mathbf{r}) = F(x,y) = \cos^{1/2}[\pi(r_b - r_f)/(L_r - 2r_f)]$ for $r_b \geqslant r_f$ and $F(\mathbf{r}) = F(x,y) = 1$ for $r_b \leqslant r_f$. Here $r_b = \sqrt{x^2 + y^2/\varepsilon^2}$, $r_f = 2.1x_q$ with $x_q = E_0/\omega^2$, and $L_r/2 = r_f + 50$ a.u. with $L_r \leqslant L_x$. In the inner region, the wave function $\Psi_{\text{in}}(\mathbf{r},t)$ propagates with the complete Hamiltonian $H(t)$. In the outer region, the time evolution of the wave function $\Psi_{\text{out}}(\mathbf{r},t)$ is carried out in momentum space with the Hamiltonian of the free electron in the laser field. The mask function is applied at each time interval of 0.5 a.u. and the new fractions of the outer wave function obtained are added to the momentum-space wave function $\tilde{\Psi}_{\text{out}}(\mathbf{r},t)$ from which we obtain the PMD. Then the offset angle θ is obtained with a Gaussian fit of the angle distribution. Relevant 2D results are presented in Figs. 1–7.

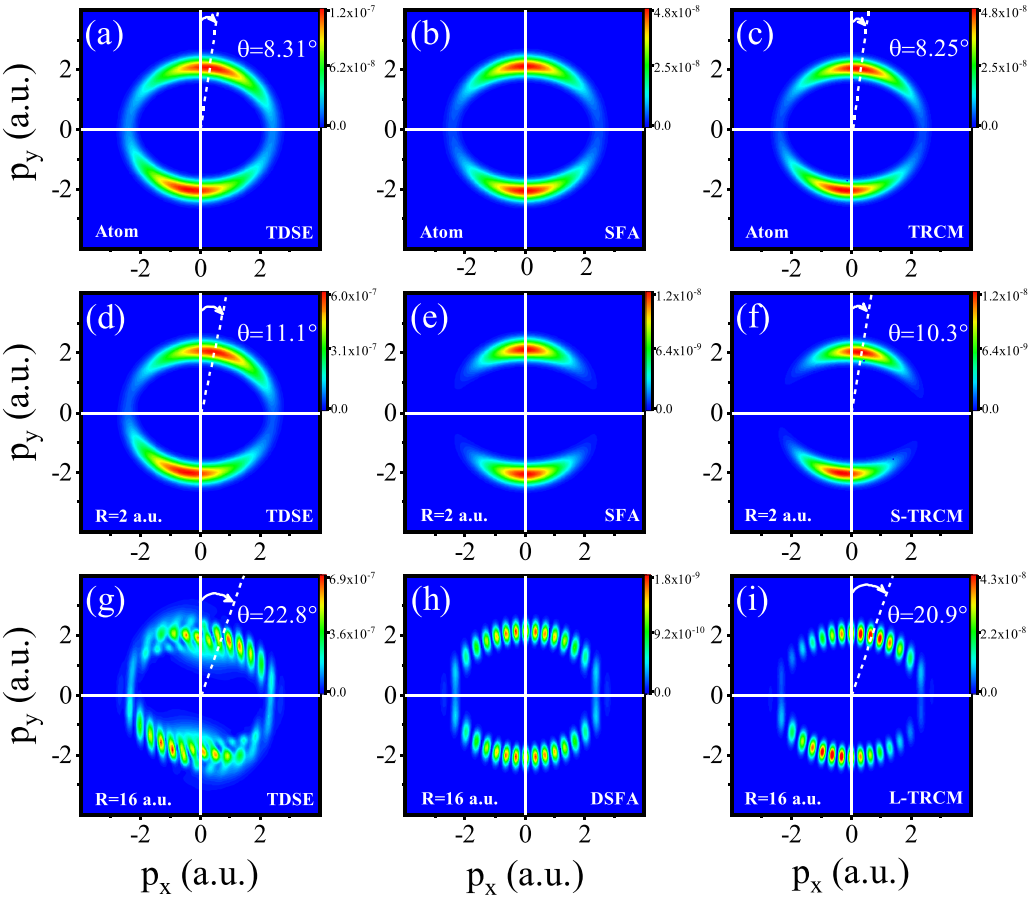

FIG. 2. PMDs of (a)–(c) the model atom, (d)–(f) 2D H_2^+ with $R = 2$ a.u., and (g)–(i) 2D H_2^+ with $R = 16$ a.u., obtained with different methods: (a), (d), and (g) the TDSE, (b) and (e) the SFA, (h) the DSFA, (c) the TRCM method, (f) the S-TRCM method, and (i) the L-TRCM method. The nonzero offset angle θ of the PMD is also indicated in each panel. The laser parameters are $I = 1\times10^{15}$ W/cm^2, $\lambda = 800$ nm, and $\varepsilon = 0.87$.

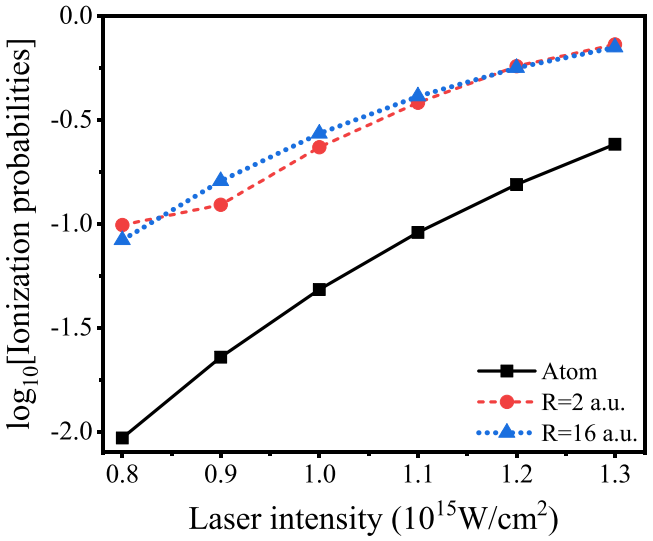

FIG. 3. Comparison of ionization probabilities for the model atom (black squares), 2D H_2^+ with $R = 2$ a.u. (red circles), and 2D H_2^+ with $R = 16$ a.u. (blue triangles), obtained by the TDSE at different laser intensities. The laser wavelength is $\lambda = 800$ nm and the ellipticity is $\varepsilon = 0.87$.

We also extend our TDSE simulations to three-dimensional (3D) cases for H_2^+ with different internuclear distances. In 3D cases, we also assume that the laser polarization is along the x axis and the molecular axis is located in the xy plane with an angle θ' to the x axis, as in 2D cases. The 3D potential used here has the form $V(\mathbf{r}) = -Z/\sqrt{r_1^2+\xi} - Z/\sqrt{r_2^2+\xi}$, with $r_{1,2}^2 = (x \pm R/2\cos\theta')^2 + (y \pm R/2\sin\theta')^2 + z^2$ and $\xi = 0.5$. For different cases of R, we also fix the value of the ionization potential at $I_p = 1.11$ a.u. with adjusting the effective charge Z. For example, $Z = 2.068$ for $R = 16$ a.u., $Z = 2.085$ for $R = 18$ a.u., and $Z = 2.101$ for $R = 20$ a.u. The grid size in three dimensions is $L_x\times L_y\times L_z = 358.4\times358.4\times51.2$ a.u. with $\triangle x = \triangle y = 0.7$ a.u. and $\triangle z = 0.8$ a.u. The mask function used here is similar to that introduced in Ref. [41]. The PMD with respect to (p_x, p_y) is obtained with the integral of the 3D momentum distribution for the component of p_z [42]. Relevant 3D results are presented in Fig. 8.

B. Strong-field models

1. SFA

According to the SFA [36], the time-dependent wave function $|\Psi(t)\rangle$ for an atom or a molecule with small R interacting

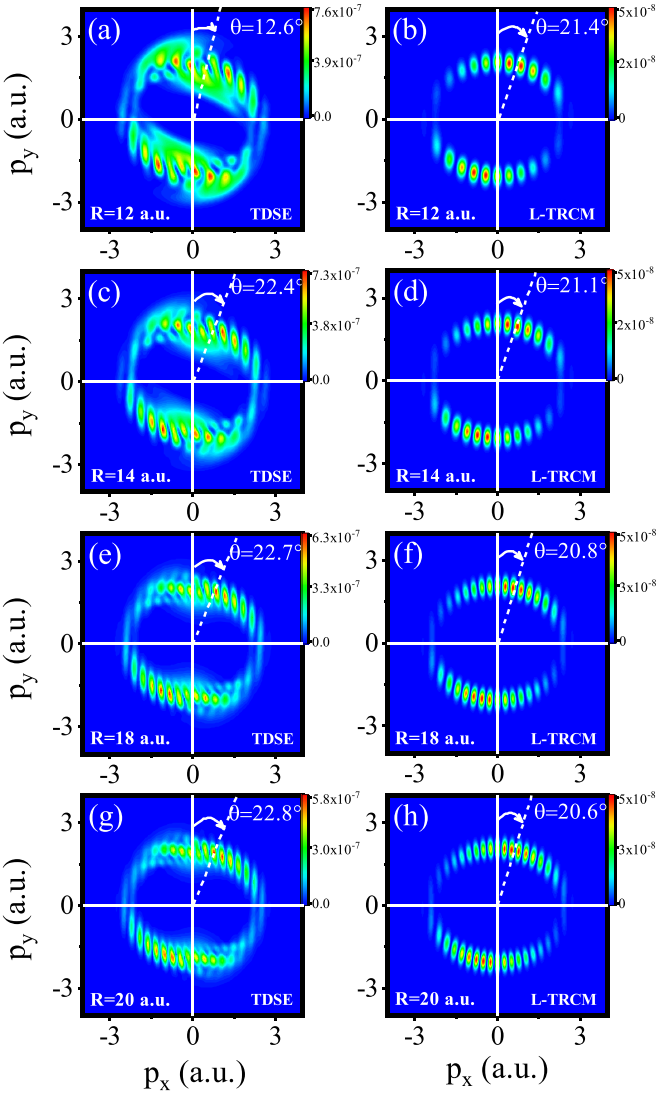

FIG. 4. PMDs of 2D H_2^+ with (a) and (b) $R = 12$ a.u., (c) and (d) $R = 14$ a.u., (e) and (f) $R = 18$ a.u., and (g) and (h) $R = 20$ a.u., obtained with the TDSE (left column) and the L-TRCM model (right column). The offset angle θ of the PMD is also indicated in each panel. The laser parameters are $I = 1\times10^{15}$ W/cm^2, $\lambda = 800$ nm, and $\varepsilon = 0.87$.

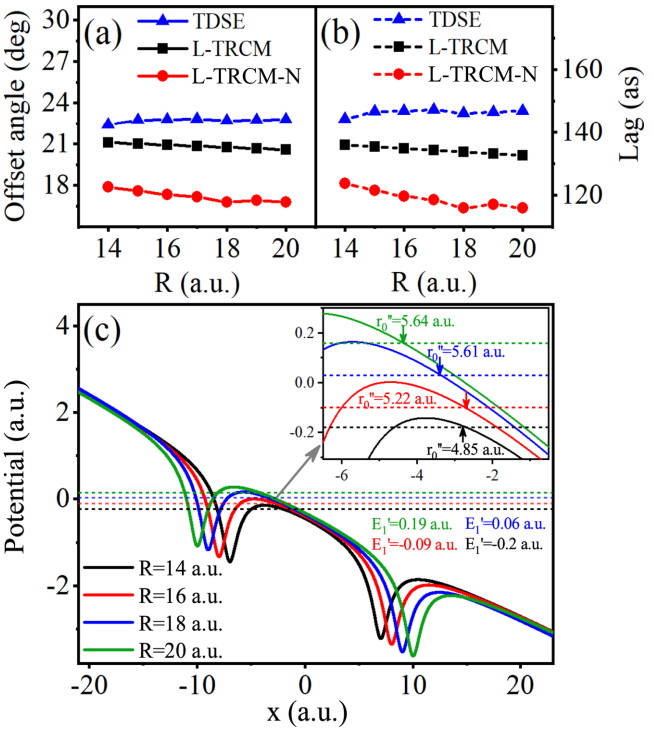

FIG. 5. Comparison of the offset angle and time lag predicted by different methods for different internuclear distances R. (a) Offset angles of 2D H_2^+ predicted by the TDSE, the L-TRCM model, and the L-TRCM model neglecting the cos term in Eq. (16) (L-TRCM-N model) for different R. (b) Time lags calculated with the expression of $\tau = \varepsilon\theta/\omega$ for the angles of the TDSE and the L-TRCM model in (a) and with the expression of Eq. (29) corresponding to the angles of the L-TRCM-N model in (a). (c) Sketch of the laser-dressed potential $V'(\mathbf{r}) = V(\mathbf{r}) - E_0 x$ (solid curves) for 2D H_2^+ with different R at $y = 0$. The horizontal dashed lines represent the dressed-up energy E_1' for 2D H_2^+ with $R = 14$ a.u. (black curves), $R = 16$ a.u. (red curves), $R = 18$ a.u. (blue curves), and $R = 20$ a.u. (green curves). The inset in (c) shows the enlarged results of the exit positions r_0'' of 2D H_2^+ with different R [also see Fig. 1(b) for the specific definition of r_0'']. The laser parameters are $I = 1\times10^{15}$ W/cm^2, $\lambda = 800$ nm, and $\varepsilon = 0.87$.

with a strong laser field can be written as

$$|\Psi(t)\rangle = e^{iI_p t}\left(a(t)|0\rangle + \int d^3\mathbf{p}\, c(\mathbf{p},t)|\mathbf{p}\rangle\right), \tag{2}$$

where $|0\rangle$ and $|\mathbf{p}\rangle$ denote the field-free ground state and continuum state of the system, respectively, I_p is the ionization potential of the ground state, the term $a(t)$ is the ground-state amplitude, and the term $c(\mathbf{p},t)$ is the amplitude of the continuum state. Assuming $a(t) \simeq 1$, the amplitude $c(\mathbf{p},t)$ at $t \to \infty$ can be expressed as [36]

$$c(\mathbf{p}) = i\int_0^{T_p} dt'\mathbf{E}(t')\cdot\mathbf{d}_i[\mathbf{p}+\mathbf{A}(t')]e^{-iS(\mathbf{p},t')}, \tag{3}$$

with $c(\mathbf{p}) \equiv c(\mathbf{p}, t\to\infty)$. Here the term $S(\mathbf{p},t') = \int_{t'}\{[\mathbf{p}+\mathbf{A}(t'')]^2/2 + I_p\}dt''$ is the semiclassical action and T_p is the length of the total pulse. The term $\mathbf{d}_i(\mathbf{v}) = \langle\mathbf{v}|\mathbf{r}|0\rangle$ denotes the dipole matrix element for the bound-free transition. The term $\mathbf{A}(t) = -\int^t \mathbf{E}(t')dt'$ is the vector potential of the electromagnetic field.

For the laser field with high intensity and low frequency, the temporal integral in Eq. (3) can be evaluated by the saddle-point method [25,36] with solving the following equation:

$$[\mathbf{p}+\mathbf{A}(t_s)]^2/2 = -I_p. \tag{4}$$

The solution t_s of Eq. (4) is complex and can be written as $t_s = t_0 + it_x$. The real part t_0 of the saddle-point time t_s is considered as the tunneling-out time at which the electron exits the laser-Coulomb-formed barrier through tunneling. The corresponding momentum-time pair $(\mathbf{p}, t_0)$ is referred to as the electron trajectory. The corresponding amplitude of the trajectory $(\mathbf{p}, t_0)$ can be expressed as

$$F(\mathbf{p},t_0) \equiv F(\mathbf{p},t_s) \propto \{\beta\mathbf{E}(t_s)\cdot\mathbf{d}_i[\mathbf{p}+\mathbf{A}(t_s)]e^{-iS}\}, \tag{5}$$

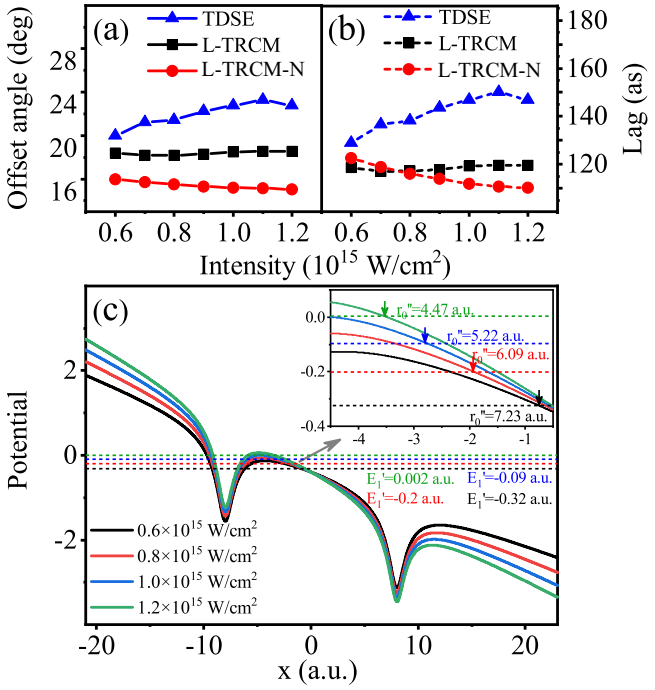

FIG. 6. Comparison of the offset angle and time lag predicted by different methods for different laser intensities I. (a) Offset angles of 2D H_2^+ predicted by the TDSE, the L-TRCM model, and the L-TRCM-N model for different I. (b) Time lags calculated with the expression of $\tau = \varepsilon\theta/\omega$ for the angles of the TDSE and the L-TRCM model in (a) and with the expression (29) corresponding to the angles of the L-TRCM-N model in (a). (c) Sketch of the laser-dressed potential $V'(\mathbf{r}) = V(\mathbf{r}) - E_0 x$ (solid curves) for 2D H_2^+ at different laser intensities with $y = 0$. The horizontal dashed lines represent the dressed-up energy E_1' for 2D H_2^+ at $I = 0.6\times10^{15}$ W/cm^2 (black curves), $I = 0.8\times10^{15}$ W/cm^2 (red curves), $I = 1.0\times10^{15}$ W/cm^2 (blue curves), and $I = 1.2\times10^{15}$ W/cm^2 (green curves). The inset in (c) shows a close-up of the results of the exit positions r_0'' of 2D H_2^+ at different I [also see Fig. 1(b) for the specific definition of r_0'']. The internuclear distance is $R = 16$ a.u., the laser wavelength is $\lambda = 800$ nm, and the ellipticity is $\varepsilon = 0.87$.

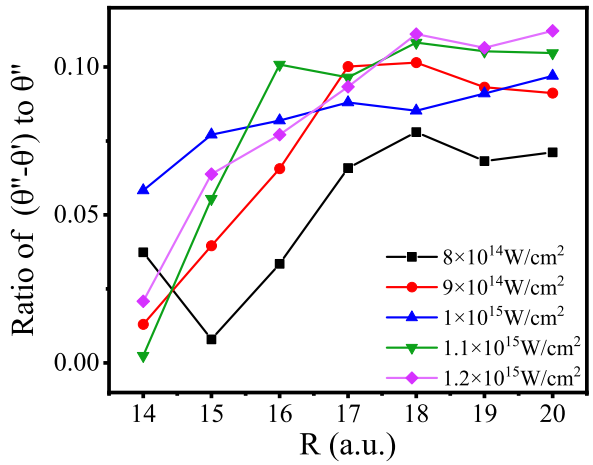

FIG. 7. Comparison of the ratios of the difference between the offset angle θ'' predicted by the TDSE and the offset angle θ' predicted by the L-TRCM model to θ'' at different internuclear distances R and laser intensities I for 2D H_2^+. The laser wavelength is $\lambda = 800$ nm and the ellipticity is $\varepsilon = 0.87$.

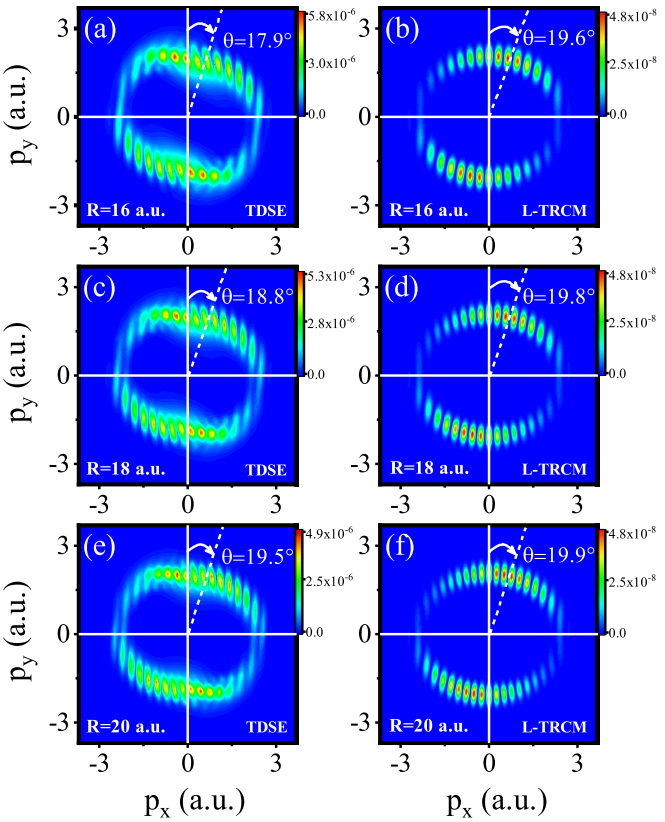

FIG. 8. PMDs of 3D H_2^+ with (a) and (b) $R = 16$ a.u., (c) and (d) $R = 18$ a.u., and (e) and (f) $R = 20$ a.u., obtained with the TDSE (left column) and the L-TRCM model (right column). The offset angle θ of the PMD is also indicated in each panel. The laser parameters are $I = 1\times10^{15}$ W/cm^2, $\lambda = 800$ nm, and $\varepsilon = 0.87$.

with $S \equiv S(\mathbf{p}, t_s)$ and $\beta \equiv [1/\det(t_s)]^{1/2}$. The term $\det(t_s)$ in the definition of β is the determinant of the matrix formed by the second derivatives of the action [36]. The whole amplitude for a photoelectron with a momentum $\mathbf{p}$ can be written as

$$c(\mathbf{p}) \propto \sum_{t_s} F(\mathbf{p}, t_s). \tag{6}$$

The sum runs over all possible saddle points.

For cases of molecules with small R, the specific form of the dipole matrix element in Eq. (5) can be written as

$$\mathbf{d}_i(\mathbf{v}) = \cos\left(\mathbf{v}\cdot\frac{\mathbf{R}}{2}\right)\mathbf{d}_a(\mathbf{v}), \tag{7}$$

with $\mathbf{v} = \mathbf{p} + \mathbf{A}(t_s)$. The term $\mathbf{d}_a(\mathbf{v}) = \langle\mathbf{v}|\mathbf{r}|\phi_a(\mathbf{r})\rangle$ denotes the atomic dipole moment and $|\phi_a(\mathbf{r})\rangle$ is the atomic ground-state wave function. By solving Eq. (4) we have $v = p + A(t_s) \approx \pm i\sqrt{2I_p}$. This imaginary momentum in the cos term in Eq. (7) does not cause interference [43]. For $1s$ orbits related to long-range Coulomb potentials, the dipole $|\mathbf{d}_a(\mathbf{v})|$ with imaginary momentum $\mathbf{v}$ can be considered close to a constant factor for different $\mathbf{p}$. Then the amplitude $F(\mathbf{p}, t_0)$ of Eq. (5) can be further approximated as $F(\mathbf{p}, t_0) \sim \cos\{[\mathbf{p} + \mathbf{A}(t_s)]\cdot\mathbf{R}/2\}e^{-iS}$ [44,45]. In this paper we evaluate the SFA amplitude with this expression. For molecules with large R, the situation is different, as will be discussed below.

2. Developed SFA

For the case of large R, due to the strong coupling between the ground state and the first excited state, the contribution of the first excited state also needs to be considered in the SFA [46]. In this case the assumptions in the developed SFA (DSFA) are as follows. (i) Except for the ground state $|0\rangle$ and the first excited state $|1\rangle$, the contribution of other bound states can be neglected. (ii) The depletion of these two lowest states can be neglected. (iii) In the continuum, the electron can be described using the plane wave $|\mathbf{p}\rangle$, with the omission of the Coulomb effect. Then the time-dependent wave function can be approximated as [47]

$$|\Psi(t)\rangle = e^{iI_p t}\left(a(t)|0\rangle + b(t)|1\rangle + \int d^3\mathbf{p}\, c(\mathbf{p},t)|\mathbf{p}\rangle\right). \quad (8)$$

Inserting Eq. (8) into the Schrödinger equation $i\dot{\Psi}(t) = H(t)\Psi(t)$, one obtains the amplitude $c(\mathbf{p},t)$ of the corresponding continuum state at $t \to \infty$, which can be expressed as [32,34]

$$c(\mathbf{p}) = i\int_0^{T_p} dt' \mathbf{E}(t')\cdot\mathbf{d}_f[\mathbf{p}+\mathbf{A}(t')]e^{-iS(\mathbf{p},t')}, \quad (9)$$

where $c(\mathbf{p}) \equiv c(\mathbf{p}, t\to\infty)$ and

$$\mathbf{d}_f(\mathbf{v}) = a(t')\mathbf{d}_0(\mathbf{v}) + b(t')\mathbf{d}_1(\mathbf{v}), \quad (10)$$

with $\mathbf{d}_m(\mathbf{v}) = \langle\mathbf{v}|\mathbf{r}|m\rangle$ and $m = 0, 1$. Assuming that the ionization potential of the ground state is equal to that of the first excited state and that $a(0) = 1$ and $b(0) = 0$, the solutions for the amplitude $a(t)$ of the ground state and the amplitude $b(t)$ of the first excited state under the two-level approximation can be written as [34]

$$a(t) = \tfrac{1}{2}(e^{i\mathbf{A}(t)\cdot\mathbf{d}_{01}} + e^{-i\mathbf{A}(t)\cdot\mathbf{d}_{01}}), \quad (11)$$

$$b(t) = \tfrac{1}{2}(e^{i\mathbf{A}(t)\cdot\mathbf{d}_{01}} - e^{-i\mathbf{A}(t)\cdot\mathbf{d}_{01}}). \quad (12)$$

Here the term $\mathbf{d}_{01} = \langle 0|\mathbf{r}|1\rangle$ denotes the dipole transition matrix element between the ground state and the first excited state. As the internuclear distance R is large enough, $\mathbf{d}_{01} \approx \mathbf{R}/2$, where $\mathbf{R}$ is the vector between these two cores of the molecule. Then the temporal integral in Eq. (9) can also be evaluated by the saddle-point method with solving Eq. (4). The corresponding complex amplitude $F(\mathbf{p}, t_0)$ for the electron trajectory $(\mathbf{p}, t_0)$ can be expressed as

$$F(\mathbf{p},t_0) \equiv F(\mathbf{p},t_s) \propto \{\beta\mathbf{E}(t_s)\cdot\mathbf{d}_f[\mathbf{p}+\mathbf{A}(t_s)]e^{-iS}\}. \quad (13)$$

A simple comparison between Eqs. (5) and (13) shows that they differ only for the dipole matrix element.

Under the approximation of the linear combination of atomic orbitals and molecular orbitals, the wave functions of the ground state $|0\rangle$ and the first excited state $|1\rangle$ of $H_2{}^+$ with large R can be written as [37]

$$|0\rangle = c_0[|\phi_a(\mathbf{r}-\mathbf{R}/2)\rangle + |\phi_a(\mathbf{r}+\mathbf{R}/2)\rangle], \quad (14)$$

$$|1\rangle = c_0[|\phi_a(\mathbf{r}-\mathbf{R}/2)\rangle - |\phi_a(\mathbf{r}+\mathbf{R}/2)\rangle]. \quad (15)$$

Here the term $c_0 = \sqrt{2}/2$ is the normalization factor. Then the dipole matrix element in Eq. (13) can be written as

$$\mathbf{d}_f(\mathbf{v}) = \cos\left(\mathbf{p}\cdot\frac{\mathbf{R}}{2}\right)\mathbf{d}_a(\mathbf{v}). \quad (16)$$

Instead of the instantaneous velocity $\mathbf{v} = \mathbf{p} + \mathbf{A}(t_s)$, only the drift momentum $\mathbf{p}$ appears in the cos term in Eq. (16). This is different from Eq. (7) for molecules with small R. It is worth noting that because the drift momentum $\mathbf{p}$ is a real number, the term $\cos(\mathbf{p}\cdot\mathbf{R}/2)$ in Eq. (16) will cause interference in the process of tunneling ionization. Considering the interference effect, the amplitude $F(\mathbf{p}, t_0)$ of Eq. (13) can be further approximated as $F(\mathbf{p}, t_0) \sim \cos(\mathbf{p}_k\cdot\mathbf{R}/2)e^{-iS}$, with $\mathbf{p}_k/|\mathbf{p}_k| = \mathbf{p}/|\mathbf{p}|$ and $p_k = |\mathbf{p}_k| = \sqrt{\mathbf{p}^2 + 2I_p}$, which takes into consideration the Coulomb correction [42]. In this paper we use $\cos(\mathbf{p}_k\cdot\mathbf{R}/2)e^{-iS}$ to evaluate the DSFA amplitude.

By inserting the expressions of $a(t)$, $b(t)$, $|0\rangle$, and $|1\rangle$ into Eq. (8), the wave function can be written as

$$\begin{aligned}|\Psi(t)\rangle = {}& \frac{\sqrt{2}}{2}e^{i[I_p t+\mathbf{A}(t)\cdot(\mathbf{R}/2)]}|\phi_a(\mathbf{r}-\mathbf{R}/2)\rangle \\ &+ \frac{\sqrt{2}}{2}e^{i[I_p t-\mathbf{A}(t)\cdot(\mathbf{R}/2)]}|\phi_a(\mathbf{r}+\mathbf{R}/2)\rangle \\ &+ e^{iI_p t}\int d^3\mathbf{p}\, c(\mathbf{p},t)|\mathbf{p}\rangle. \end{aligned} \quad (17)$$

Equation (17) shows that for the stretched system with large R, bound electrons can be considered to be located at these two laser-dressed states $|\phi_a(\mathbf{r}-\mathbf{R}/2)\rangle$ and $|\phi_a(\mathbf{r}+\mathbf{R}/2)\rangle$. They correspond to the states of two atoms which both have the ionization potential I_p and are placed at positions $\pm\mathbf{R}/2$ deviated from the coordinate origin. This deviation gives rise to the dressed phases of $I_p t + \mathbf{A}(t)\cdot\mathbf{R}/2$ and $I_p t - \mathbf{A}(t)\cdot\mathbf{R}/2$, respectively [32,34]. Tunneling ionization events occur from these two states along their respective dressed energies, and the two ionization channels interfere with each other. Besides interference, these two channels can also be coupled together by the Coulomb effect, as will be discussed below.

Let us consider the time region around the peak time t_p of the laser field with $E_x(t_p) \approx E_0$ at which the tunnel event mainly occurs. Around the peak time t_p, we have $A_x(t) \approx -E_0 t$. In this paper we assume that the molecular axis is parallel to the major axis of the laser polarization ellipse with $\theta' = 0^o$. Then the dressed energies E_1' and E_2' can be written as

$$E_1' \approx -\left(I_p - E_0\frac{R}{2}\right), \quad (18)$$

$$E_2' \approx -\left(I_p + E_0\frac{R}{2}\right). \quad (19)$$

In Fig. 1(b) we use Eqs. (18) and (19) to analyze the mechanism of tunneling ionization related to dressed states for molecules with large R. One of the limitations in the SFA and DSFA is that the Coulomb potential is neglected. Next we further discuss strong-field models that consider the Coulomb effect.

C. Coulomb-included strong-field models

A Coulomb-included strong-field model has been developed to describe tunneling ionization of electrons in atoms and molecules with small R; this model is called the tunneling-response classical-motion (TRCM) model [41]. According to the TRCM model, the process of strong-field ionization can be divided into three steps of tunneling, response, and

classic motion. These steps can be described with saddle-point [25,36], semiclassical [41], and simple-man [7,48] theories, respectively. This model arises from the SFA [36] but considers the Coulomb effect [39,49,50]. The SFA mapping relation between the drift momentum $\mathbf{p}$ and the tunneling-out time t_0 can be written as

$$\mathbf{p} \equiv \mathbf{p}(t_0) = \mathbf{v}(t_0) - \mathbf{A}(t_0). \tag{20}$$

The term $\mathbf{v}(t_0) = \mathbf{p} + \mathbf{A}(t_0)$ denotes the exit velocity of the photoelectron at the exit position [50]

$$\mathbf{r}_0 \equiv \mathbf{r}(t_0) = \mathrm{Re}\left(\int_{t_0+it_x}^{t_0} [\mathbf{p} + \mathbf{A}(t')]dt'\right). \tag{21}$$

To consider the influence of the Coulomb potential on ionization, the TRCM model assumes that at the tunnel exit $\mathbf{r}(t_0)$, the tunneling electron with the drift momentum $\mathbf{p}$ is still located at a quasibound state, which approximately agrees with the virial theorem. A small period of time τ is needed for the tunneling electron to evolve from the quasibound state into an ionized state. Then it is free at the time $t_i = t_0 + \tau$ with the Coulomb-included drift momentum $\mathbf{p}'$. This time τ can be understood as the response time of the electron to light in laser-induced photoelectric effects and manifests as the Coulomb-induced ionization time lag in strong-field ionization [51,52]. The mapping between the drift momentum $\mathbf{p}'$ and the ionization time t_i in the TRCM model can be expressed as

$$\mathbf{p}' \equiv \mathbf{p}'(t_i) = \mathbf{v}(t_0) - \mathbf{A}(t_i). \tag{22}$$

Below we will introduce the expressions of lag τ for atoms and molecules with small R and explore the expression of lag τ for the case of large R.

1. Expressions of τ for atoms

According to the TRCM model for atoms, at the tunneling-out time t_0, the tunneling electron is still located in a quasibound state ψ_b, which approximately agrees with the virial theorem [41]. The average potential energy of this state is $\langle V(\mathbf{r})\rangle \approx V(\mathbf{r}(t_0))$ and the average kinetic energy is $\langle \mathbf{v}^2/2\rangle = n_f\langle v_x^2/2\rangle \approx -V(\mathbf{r}(t_0))/2$. Semiclassical treatment of the quasibound state gives a velocity $|\mathbf{v}_i| = \sqrt{\langle v_x^2\rangle} \approx \sqrt{|V(\mathbf{r}(t_0))|/n_f}$, which is opposite to the direction of the position vector $\mathbf{r}(t_0)$ and reflects the basic symmetry requirement of the Coulomb potential on the electronic bound state. This state implies a bound wave packet composed of a series of high-energy bound eigenstates of field-free Hamiltonian H_0 here. A small period of time τ is needed for the tunneling electron to obtain the opposite velocity $-\mathbf{v}_i$ from the laser field in order to break this symmetry. This implies $|\mathbf{E}(t_0)|\tau \approx |\mathbf{v}_i|$. In the elliptically polarized laser field, the time lag τ can be evaluated with the expression

$$\tau \approx \sqrt{|V_a(\mathbf{r}(t_0))|/n_f}/|\mathbf{E}(t_0)|. \tag{23}$$

Here $|\mathbf{E}(t_0)| = \sqrt{(E_0 \sin\omega t_0)^2 + (E_1 \cos\omega t_0)^2}$ is the amplitude of the laser electric field $\mathbf{E}(t)$ at time t_0. The exit position $\mathbf{r}_0 \equiv \mathbf{r}(t_0)$ can be evaluated using Eq. (21). The term n_f is the dimension of the system studied. For 2D cases studied we have $n_f = 2$, and for 3D cases we have $n_f = 3$. In single-active electron approximation, the potential $V(\mathbf{r})$ of a hydrogenlike atom at the exit position $\mathbf{r}_0$ can be considered to have the form $V_a(\mathbf{r}(t_0)) \equiv V_a(\mathbf{r}_0) = -Z'/\mathbf{r}_0$. Here Z' is the effective charge. For comparison with TDSE simulations, the effective charge Z' can be chosen as that used in simulations. For comparison with experiments, the value of Z' can be evaluated with $Z'_a \approx \sqrt{2I_p}$. Once the lag τ is obtained, using Eq. (22), one can obtain the Coulomb-included drift momentum $\mathbf{p}' = \mathbf{v}(t_0) - \mathbf{A}(t_i)$, with $t_i = t_0 + \tau$. Assuming that the amplitude $F(\mathbf{p}', t_i)$ for the Coulomb-included electron trajectory $(\mathbf{p}', t_i)$ is equivalent to the corresponding amplitude $F(\mathbf{p}, t_0)$ for the SFA trajectory $(\mathbf{p}, t_0)$, the amplitude $F(\mathbf{p}', t_i)$ can be written as

$$F(\mathbf{p}', t_i) \equiv F(\mathbf{p}, t_0) \propto \{\beta \mathbf{E}(t_s)\cdot \mathbf{d}_a[\mathbf{p} + \mathbf{A}(t_s)]e^{-iS}\}, \tag{24}$$

with $S \equiv S(\mathbf{p}, t_s)$ and $\beta \equiv [1/\det(t_s)]^{1/2}$. The amplitude $F(\mathbf{p}', t_i)$ of Eq. (24) can be further approximated as $F(\mathbf{p}', t_i) \sim e^{-iS}$. In this paper we use e^{-iS} to evaluate the TRCM model amplitude for atoms. In this way, we can obtain the Coulomb-included PMD directly from the SFA without needing to solve the Newton equation including both the electric force and the Coulomb force. Then the offset angle θ is obtained with a Gaussian fit of the angle distribution. Below, the TRCM model with the lag τ calculated by Eq. (23) is referred to as the A-TRCM model.

2. Expressions of τ for molecules with small R

For molecules with small R, the situation is different. In Fig. 1(a) we plot the laser-dressed and laser-free potential function curves for 2D H_2^+ with $R = 2$ a.u. and a model atom with similar I_p to H_2^+ at the peak time t_p of the laser field. One can see from Fig. 1(a) that the barrier formed by the laser field and the two-center Coulomb potential of H_2^+ is lower and narrower than the atomic single-center one. Accordingly, the tunnel exit for the molecule is nearer to the nuclei than the atomic one and the tunneling electron of the molecule feels a stronger Coulomb force. To overcome this stronger Coulomb force remaining at the tunnel exit, a longer response time τ is required for the tunneling electron of the molecule to obtain enough impulse from the laser field [53]. Next we discuss the expression of time lag τ for molecules with small R in detail.

First, at the tunnel exit, which is of the order of 10 a.u. for general laser parameters used in experiments, one can consider that the tunneling electron of the molecule is still located in a quasibound state, which consists of high-energy bound eigenstates of the molecule and also agrees approximately with the virial theorem. This implies that the expression $|\mathbf{E}(t_0)|\tau \approx |\mathbf{v}_i| \approx \sqrt{|V(\mathbf{r}(t_0))|/n_f}$ still holds for molecules. The remaining question is how the form of the potential $V(\mathbf{r}(t_0))$ can be determined for molecules. Second, as seen in Fig. 1(a), the atom and the molecule have different forms of Coulomb potential. Therefore, (i) the exit positions of the atom and the molecule differ from each other. The exit position is about 0.75 a.u. (approximately $R/2$) smaller for the molecule with $R = 2$ a.u. than for the atom. (ii) The left part of the molecular potential is dressed up by the laser field, with an energy shift of $E_d = E_0(R/2)$. This potential-dressed phenomenon around the nucleus disappears for the atom. This phenomenon implies that the molecule with the dressed ionization potential $I'_p = I_p - E_d$ is somewhat easier to ionize than the atom. With the above discussion of (i) and

(ii), the exit position of the molecule with small R at the peak time t_p can be approximated as $r_0' \approx I_p'/E_0 - R/2 \approx r_p - R$ [53]. Here $r_p \approx I_p/E_0$ denotes the classic estimation of the exit position of the electron within an atom which ionizes in the time region around the peak time t_p of the laser fundamental field $E_x(t)$ [8]. We assume that the correction R to this exit position is applicable for any time t_0, and the two-center Coulomb potential of the molecule at the tunnel exit can also be approximated with a single-center one corresponding to a model atom. The expression of the time lag τ for molecules with small R can be written as

$$\tau \approx \sqrt{|V_s(\mathbf{r}'(t_0))|/n_f}/|\mathbf{E}(t_0)|. \tag{25}$$

Here $|\mathbf{r}'(t_0)| \equiv r_0' = |\mathbf{r}_0| - r_d$ is the corrected exit position at time t_0, with a correction of $r_d = R$ and where $\mathbf{r}_0$ is the SFA prediction of the exit position which can be evaluated by Eq. (21). The potential $V(\mathbf{r})$ for the case of small R at the exit position $\mathbf{r}'(t_0)$ has the form $V_s(\mathbf{r}'(t_0)) = -Z'/|\mathbf{r}'(t_0)|$. Here Z' is the whole effective charge of the molecule. For comparison with TDSE simulations, the whole effective charge Z' can be chosen as that used in simulations. For example, for the 2D H_2^+ case with $R = 2$ a.u. that we study in the present paper, we have $Z' = 2$. For comparison with experiments, the value of Z' can be evaluated with $Z_m' \approx I_p\sqrt{(R/2)^2 + Z_a'^2/I_p^2}$ for molecules with the internuclear distance R. The expression of Z_m' is obtained assuming that $I_p \approx Z_a'/\sqrt{\zeta_0^2}$ for the companion atom and $I_p \approx Z_m'/\sqrt{(R/2)^2 + \zeta_0^2}$ for the molecule. Here ζ_0 is a constant factor. For convenience, in the following, the TRCM model with the lag τ calculated by Eq. (25) is called the S-TRCM model.

In the S-TRCM model, it is still considered that the amplitude $F(\mathbf{p}', t_i)$ for the Coulomb-included electron trajectory $(\mathbf{p}', t_i)$ is equivalent to the corresponding amplitude $F(\mathbf{p}, t_0)$ for the SFA trajectory $(\mathbf{p}, t_0)$. Then the amplitude $F(\mathbf{p}', t_i)$ can be written as

$$F(\mathbf{p}', t_i) \equiv F(\mathbf{p}, t_0) \propto \{\beta \mathbf{E}(t_s) \cdot \mathbf{d}_i[\mathbf{p} + \mathbf{A}(t_s)]e^{-iS}\}. \tag{26}$$

The dipole matrix element $\mathbf{d}_i(\mathbf{v})$ is represented by Eq. (7). The amplitude $F(\mathbf{p}', t_i)$ of Eq. (26) can be further approximated as $F(\mathbf{p}', t_i) \sim \cos\{[\mathbf{p} + \mathbf{A}(t_s)] \cdot \mathbf{R}/2\}e^{-iS}$ with $p + A(t_s) \approx \pm i\sqrt{2I_p}$. In this paper we use $\cos\{[\mathbf{p} + \mathbf{A}(t_s)] \cdot \mathbf{R}/2\}e^{-iS}$ to evaluate the TRCM model amplitude for molecules with small R. Then the offset angle θ is obtained with a Gaussian fit of the angle distribution.

Next we discuss extending the TRCM model to molecules with large R.

3. Expressions of τ for molecules with large R

In Fig. 1(b) we plot the laser-free and laser-dressed potentials for the case of $R = 16$ a.u. of 2D H_2^+ at the peak time t_p of the laser field. One can observe that, in this case, the laser-free Coulomb potential shows two separate wells. Accordingly, the laser-dressed Coulomb potential shows two separate barriers: one dressed up near the left nucleus and another dressed down near the right nucleus. On the other hand, the DSFA model discussed above tells us that, due to charge resonance, the ionization of molecules with large R occurs from the laser-dressed states along the energies of E_1' and E_2', respectively. These two energies are associated with the dressed-up and the dressed-down barriers, respectively, as indicated by the horizontal arrows in Fig. 1(b). Because the dressed-up potential barrier on the left is influenced by the atomic nucleus on the right, the part of the dressed-up barrier above the horizontal line of E_1' is lower and narrower than the dressed-down barrier above the horizontal line of E_2'. Therefore, electrons will tend to tunnel through the dressed-up barrier with a smaller exit position. In other words, for molecules with large R and the ionization potential I_p, the ionization event mainly occurs around the dressed-up barrier. This ionization phenomenon is somewhat similar to that of an atom with similar I_p but a smaller exit position. In this case, we can also assume that at the tunnel exit, the tunneling electron is still located at a quasibound state ψ_b which approximately agrees with the virial theorem, and the expression $|\mathbf{E}(t_0)|\tau \approx |\mathbf{v}_i| \approx \sqrt{|V(\mathbf{r}(t_0))|/n_f}$ still holds for molecules with large R. However, for the current situation of large R, it may be necessary to make slight corrections to the above expression in order to quantitatively compare the model predictions with TDSE results. We will return to this point later. Next we further discuss the form of the potential $V(\mathbf{r}(t_0))$ in the above expression for molecules with large R.

For molecules with small R, according to the discussion in Sec. II C 2, the exit position $r_0' = |\mathbf{r}_0| - r_d$, with $r_d = R$, is smaller than the atomic one $|\mathbf{r}_0|$ at the same I_p. The discussion of Fig. 1(b) shows that this situation also holds for molecules with large R. We determine the exit position r_0'' for cases of large R directly from the laser-dressed potential, as shown in Fig. 1(b). Specifically, for $E_x(t) < 0$, the exit position near the left nucleus can be approximately calculated using

$$V(x, y_0) - E_0 x = -[I_p - E_0(R/2)] \tag{27}$$

and the exit position near the right nucleus can be calculated using

$$V(x, y_0) - E_0 x = -[I_p + E_0(R/2)]. \tag{28}$$

Here $V(x, y) \equiv V(\mathbf{r})$ is the Coulomb potential used in our TDSE simulations and $y_0 = 0$. The coordinates x_2 and x_4 in Fig. 1(b) are solutions of Eqs. (27) and (28) and correspond to the exit positions of the dressed-up and the dressed-down barriers, respectively. As discussed above, electrons tend to tunnel through the dressed-up barrier with a smaller exit position. This smaller position can be represented as $r_0'' = |x_2 - x_1|$, with x_1 relating to the position of the left nucleus. The situation is similar for $E_x(t) > 0$. We consider that the correction for the exit position at the peak time t_p is $r_d = r_p - r_0''$, with $r_p \approx I_p/E_0$, and assume that this correction holds for any time t_0. Then, for molecules with large R, the time lag τ can be expressed as

$$\tau \approx k_f\sqrt{|V_l(\mathbf{r}'(t_0))|/n_f}/|\mathbf{E}(t_0)|. \tag{29}$$

Here $|\mathbf{r}'(t_0)| \equiv r_0' = |\mathbf{r}_0| - r_d$, with $r_d = r_p - r_0''$, is the exit position at time t_0, and the value of $\mathbf{r}_0$ can be evaluated by Eq. (21). Similar to the case of small R, the potential $V(\mathbf{r})$ for the case of large R at the exit position $\mathbf{r}'(t_0)$ can be considered to have the form of $V_l(\mathbf{r}'(t_0)) = -Z'/|\mathbf{r}'(t_0)|$. Here Z' is the whole effective charge as introduced in Eq. (25). The prefactor $k_f = 1.14$ in Eq. (29) considers the fact that the virial theorem holds only when the contributions of nondiagonal components to the mean potential energy $\langle\psi_b|V(\mathbf{r})|\psi_b\rangle$

are negligible. Here $|\psi_b\rangle = \sum_n a_n|n\rangle$, with $|n\rangle$ being higher bound eigenstates of the field-free Hamiltonian H_0 of the molecular system. Our numerical simulations show that nondiagonal components contribute about 30% to the mean value [54]. In other words, instead of the virial theorem, the expression of $\langle \mathbf{v}^2\rangle/2 \approx -1.3\langle V(\mathbf{r})\rangle/2$ holds. As a result, $v_i = |\mathbf{v}_i| \approx \sqrt{1.3/|V(\mathbf{r}(t_0))|/n_f} \approx 1.14\sqrt{|V(\mathbf{r}(t_0))|/n_f}$ and $\tau \approx v_i/|\mathbf{E}(t_0)| \approx 1.14\sqrt{|V(\mathbf{r}(t_0))|/n_f}/|\mathbf{E}(t_0)|$. Therefore, the nondiagonal components contribute about 14% to the Coulomb-induced velocity v_i. For atoms and molecules with small R, they have relatively small values of v_i, and the effect of nondiagonal components on v_i is not significant. However, for molecules with large R, the exit position is nearer to the nucleus and therefore the value of v_i is larger. The correction of 14% to the velocity v_i needs to be considered. In comparison with the case of $k_f = 1$, the use of $k_f = 1.14$ in Eq. (29) results in an increase of about 2° in the model prediction of the offset angle. In addition, for comparison with TDSE simulations, the whole effective charge Z' can be chosen as that used in simulations. For comparison with experiments, one can determine the value of Z' at the equilibrium separation R of the studied molecular system with the expression of $Z'_m \approx I_p\sqrt{(R/2)^2 + Z_a'^2/I_p^2}$, as in the case of small R discussed in Sec. II C 2. Below, the TRCM model with the lag τ calculated by Eq. (29) will be termed the L-TRCM model.

By assuming that for an arbitrary DSFA electron trajectory $(\mathbf{p}, t_0)$, the Coulomb potential does not influence the corresponding complex amplitude $F(\mathbf{p}, t_0)$, we obtain the L-TRCM model amplitude $F(\mathbf{p}', t_i)$ for electron trajectory $(\mathbf{p}', t_i)$ directly from the DSFA one with $F(\mathbf{p}', t_i) \equiv F(\mathbf{p}, t_0)$ at τ. The amplitude $F(\mathbf{p}', t_i)$ can be written as

$$F(\mathbf{p}', t_i) \equiv F(\mathbf{p}, t_0) \propto \{\beta \mathbf{E}(t_s)\cdot \mathbf{d}'_f[\mathbf{p} + \mathbf{A}(t_s)]e^{-iS}\}. \quad (30)$$

The dipole matrix element $\mathbf{d}_f(\mathbf{v})$ is represented by Eq. (16). The amplitude $F(\mathbf{p}', t_i)$ of Eq. (30) can be further approximated as $F(\mathbf{p}', t_i) \sim \cos(\mathbf{p}'_k \cdot \mathbf{R}/2)e^{-iS}$ with $\mathbf{p}'_k/|\mathbf{p}'_k| = \mathbf{p}'/|\mathbf{p}'|$ and $p'_k = |\mathbf{p}'_k| = \sqrt{\mathbf{p}'^2 + 2I_p}$, which takes the Coulomb correction into consideration [42]. In this paper we use $\cos(\mathbf{p}'_k \cdot \mathbf{R}/2)e^{-iS}$ to evaluate the TRCM model amplitude for molecules with large R. Then the PMD of the L-TRCM model can be obtained, and the offset angle θ can be further obtained with a Gaussian fit of the angle distribution. In the following, we will show that the L-TRCM model gives a good description of the PMD of molecules with large R.

III. RESULTS AND DISCUSSION

A. Laser-dressed ionization picture

Before comparing results of the TDSE and models, we further discuss Fig. 1, which shows the basic difference between laser-dressed potentials of atoms and molecules with small and large R. This difference is related to the inherent geometric structure of the studied system. It plays an important role in the difference between ionization mechanisms of atoms and molecules with different R. When the laser-dressed potential curves for atoms and molecules with small R show a single barrier in Fig. 1(a), the laser-dressed potential curves of large R in Fig. 1(b) show two barriers near the positions of these two stretched nuclei. One barrier is dressed up and another is dressed down. As discussed in Sec. II C 3, due to the contribution of the first excited state, the molecule with large R will be ionized along the energies $E'_1 \approx -(I_p - E_0R/2)$ and $E'_2 \approx -(I_p + E_0R/2)$, as shown by the two horizontal lines in Fig. 1(b). The dressed-up barrier is related to the energy $E'_1 = -0.09$ a.u. and the dressed-down barrier is associated with the energy $E'_2 = -2.13$ a.u. The dressed energies E'_1 or E'_2 are not the actual ionization potential of the system that will appear in the saddle-point equation (4), but reflect the fact that the ionization occurs near an atomic center which is not located at the coordinate origin [33]. The part of the dressed-up barrier above the horizontal line of E'_1 is lower and narrower than the dressed-down one above the horizontal line of E'_2, as shown by the intersections of the horizontal lines and the laser-dressed potential function curves. As a result, the dressed-up barrier is preferred for the bound electron of the stretched molecule to escape through tunneling from the neighboring well. In fact, for the present case in Fig. 1(b), by solving Eqs. (27) and (28), it can be obtained that the exit position of the upper barrier relative to the position of the neighboring nucleus (i.e., the left nucleus) is $r''_0 = 5.22$ a.u. and the exit position of the lower barrier relative to the position of the neighboring nucleus (i.e., the right nucleus) is $r''_0 = 5.84$ a.u. The exit position of the potential barrier near the left nucleus is smaller than that of the right nucleus, because the left potential barrier is influenced by the right nucleus. The exit position $r''_0 = 5.22$ a.u. of the upper barrier is used to obtain the correction parameter r_d of the exit position in the L-TRCM model, which can be written as $r_d = r_p - r''_0$, with $r_p \approx I_p/E_0$. The L-TRCM model predicts an offset angle of the PMD that is similar to the TDSE one, as will be shown in Fig. 2. Therefore, our work is able to provide a concise Coulomb-included strong-field model to describe tunneling ionization of molecules with large R.

From Fig. 1(a) one can also see that the exit positions of the barriers for the model atom and H_2^+ with $R = 2$ a.u. are 6.46 and 5.71 a.u., respectively. They are also larger than $r''_0 = 5.22$ a.u., as discussed in Fig. 1(b) for the upper barrier near the left nucleus. This somewhat smaller exit position for molecules with large R than that for atoms and molecules with small R leads to a somewhat larger ionization probability for the case of large R, since tunneling is easier to occur for a narrower barrier. It also results in a larger offset angle in the PMD, since the Coulomb force felt by tunnel electrons at the tunnel exit is stronger for smaller exit positions. We will further discuss these points in Figs. 2–4.

We mention that from the blue curve of the dressed potential in Fig. 1(b), one can also understand the motion of the electron after tunneling for the case of molecules with large R. As the electronic wave packet exits the dressed-up potential barrier and moves towards the right, there is a certain probability that the electron will be recaptured by the nucleus on the right. This recapture process will induce the emission of harmonics with the largest energy E_0R. Because this process occurs around these two nuclei where the Coulomb effect is strong, harmonics emitted in this process have also high intensities, forming the so-called molecular high-order harmonic generation plateau [47].

B. Characteristics of the PMD

In the following, we first discuss ionization results for 2D cases in Figs. 2–7 and then we extend our consideration to 3D cases in Fig. 8.

In Fig. 2 we show the PMDs of 2D H_2^+ with $R = 2$ and 16 a.u. and the model atom obtained with different methods. First, the TDSE results in the left column of Fig. 2 show that the offset angle of H_2^+ with $R = 16$ a.u. in Fig. 2(g) is $\theta = 22.8^o$, while that of H_2^+ with $R = 2$ a.u. in Fig. 2(d) is $\theta = 11.1^\circ$ and the offset angle of the model atom in Fig. 2(a) is $\theta = 8.31^\circ$, that is, with similar I_p, the offset angle of the molecule with large R is far larger than that of molecules with small R and model atoms. In addition, it can be observed that the PMD of H_2^+ with $R = 16$ a.u. in Fig. 2(g) displays interference fringes, which disappear for the case of $R = 2$ a.u. The different phenomena discussed above show that electrons within atoms and molecules respond differently to ionization events when they have similar I_p but different R.

Second, the PMD predicted by the SFA and DSFA models in the middle column of Fig. 2 can reproduce some main characteristics of the corresponding PMD calculated through TDSE. As shown in Figs. 2(h) and 2(e), there are obvious interference fringes in the PMD of H_2^+ with $R = 16$ a.u., which disappear in the PMD of H_2^+ with $R = 2$ a.u. Next we will discuss further the generation of interference fringes in the PMD of molecules with large R. According to the DSFA model, for molecules with large R, the dipole matrix element can be written as $\cos(\mathbf{p}\cdot\mathbf{R}/2)\mathbf{d}_a(\mathbf{v})$, as shown in Eq. (16). The momentum $\mathbf{p}$ is the drift momentum and is real. Therefore, the term $\cos(\mathbf{p}\cdot\mathbf{R}/2)$ will cause interference in the process of tunneling ionization. The situation is different for molecules with small R. According to the SFA model for molecules with small R, the dipole matrix element can be written as $\cos(\mathbf{v}\cdot\mathbf{R}/2)\mathbf{d}_a(\mathbf{v})$, as shown in Eq. (7). Under the saddle-point approximation, the instantaneous velocity $v = p + A(t_s) \approx \pm i\sqrt{2I_p}$ is an imaginary number, which does not cause interference. This is why interference fringes appear in the PMD of molecules with large R and disappear in the case of small R. By comparing the PMD results in the left and middle columns of Fig. 2, one can know that the SFA and DSFA models disregarding the Coulomb effect cannot reproduce the offset angle of the PMD calculated by the TDSE.

Third, these TDSE results can be well reproduced by strong-field models that include the Coulomb effect, as shown in the right column of Fig. 2. For the case of the model atom in Fig. 2(c), the offset angle predicted by the A-TRCM model is $\theta = 8.25^\circ$. For the case of H_2^+ with $R = 2$ a.u. in Fig. 2(f), the offset angle predicted by the S-TRCM model is $\theta = 10.3^\circ$. These model results for the offset angle are very close to the TDSE ones. The PMD of the L-TRCM model for the case of $R = 16$ a.u. is presented in Fig. 2(i). The offset angle predicted by the L-TRCM model is $\theta = 20.9^\circ$, which is also close to the result of the TDSE in Fig. 2(g). Therefore, the model results reproduce the TDSE phenomenon that the offset angle for H_2^+ with large R is remarkably larger than that for H_2^+ with small R and that for a model atom. The discussion of constructing these TRCM models in Sec. II C and analyzing the potential function curves in Fig. 1 provide explanations for the potential mechanism of the phenomenon, namely, for H_2^+ with large R, the strong resonance between the ground state and the first excited state generates two laser-dressed states with dressed energies E_1' and E_2'. The ionization of the stretched system occurs from these two laser-dressed states. The dressed-up potential barrier related to one dressed state with energy E_1' is lower and narrower than the dressed-down barrier related to another dressed state with energy E_2'. As a result, the ionization channel characterized by tunneling of the bound electron out of the dressed-up barrier near one nucleus dominates in the ionization of the system. This channel related to the dressed-up state near one nucleus is somewhat similar to that for the ionization of an atom with a single-center Coulomb potential. The difference is that this channel near one nucleus is also influenced by another nucleus. This influence is essential for H_2^+ with large R and reflects the four-body interaction between the laser, the electron, and these two nuclei of the stretched molecule. It results in the exit position of the dressed-up barrier being smaller than that of H_2^+ with small R and that of a model atom. Therefore, at the tunnel exit, the tunneling electron for H_2^+ with large R feels a stronger Coulomb force in comparison with the cases of H_2^+ with small R and the model atom. This stronger force further induces a larger offset angle in the PMD for the case of large R. In addition, the whole effective charge Z' is also larger for cases of larger R with similar I_p. For example, in our 2D TDSE simulations, $Z' = 2$ for $R = 2$ a.u., $Z' = 3.1$ for $R = 12$ a.u., $Z' = 3.14$ for $R = 14$ a.u., $Z' = 3.17$ for $R = 16$ a.u., $Z' = 3.194$ for $R = 18$ a.u., and $Z' = 3.214$ for $R = 20$ a.u. This larger value of Z' for larger R will also induce an increase of the offset angle. Our model is able to simplify the complex four-body interaction and give a clear physical picture for the ionization of the stretched system. The ionization picture, where the electron located at a dressed-up state ionizes through tunneling out of the dressed-up barrier near one nucleus, is also supported by calculating the ionization probability, as shown in Fig. 3.

In Fig. 3 we present the 2D results of TDSE ionization probabilities for the model atom, H_2^+ with $R = 2$ a.u. and H_2^+ with $R = 16$ a.u. at different laser intensities. One can observe that the ionization probability of $R = 16$ a.u. is somewhat larger than that of $R = 2$ a.u. and is remarkably larger than that of the model atom at different laser intensities. These results agree with the analysis of laser-dressed potentials presented in Fig. 1. The part of the potential barrier above the energy along which the electron tunnels out of the barrier for the case of $R = 16$ a.u. is similar to that for $R = 2$ a.u. and is remarkably lower than that for the model atom.

To further validate our above discussion, we have also performed simulations for ionization of stretched H_2^+ at different internuclear distances R. Relevant results are presented in Fig. 4, where we plot the PMDs of 2D H_2^+ with $R = 12$, 14, 18, and 20 a.u., obtained with the TDSE and L-TRCM model. For the TDSE results in the left column of Fig. 4, it can be observed that as the internuclear distance R increases, the number of interference fringes increases. This phenomenon is reproduced by the L-TRCM model, as seen in the right column of Fig. 4. The offset angle of the TDSE for $R = 12$ a.u. is 12.6°. For other cases, these angles of the TDSE are similar around a value of 22.6°. The angles predicted by the L-TRCM

model are around a value of 21° for all cases of R. The results suggest that the L-TRCM model is more applicable for the distance R larger than 14 a.u. In fact, the PMDs of the L-TRCM model show clear interference fringes. By comparison, in addition to interference fringes, the TDSE distributions also exhibit more diverse structures, especially for the case of $R = 12$ a.u. The difference in fine structures between the TDSE and L-TRCM model results of PMD becomes smaller for larger R. The potential reason for this difference can be that (i) the description of the influence of another atomic nucleus on the exit position of the dressed-up potential barrier is not accurate enough and (ii) the expressions (11) and (12) used in the L-TRCM model are more applicable for degenerate cases which are generally satisfied when the distance R is large enough. For example, our simulations show that for cases of $R = 8$, 10, and 12 a.u., with $\Delta E/w > 10^{-5}$, the PMDs show richer structures, and a more complex theory beyond the L-TRCM model is needed to describe the process of tunneling ionization. Here ΔE is the energy difference between the first excited state and the ground state of model H_2^+ molecules with similar I_p in our simulations and $w = 0.057$ a.u. is the laser frequency used in the TDSE. For cases of intermediate distances R such as $R = 4$ and 6 a.u. with $\Delta E/w \sim 1$, a strong single-photon resonance occurs between the ground state and the first excited state. For the present cases of strong laser fields beyond the description of the Rabi approximation, it is difficult to obtain accurate analytical solutions for the amplitudes of these two states [34]. To check the applicability of the L-TRCM model and identify the different roles of charge resonance and Coulomb potential in the offset angle, we have also extended our simulations to other laser and molecular parameters, as shown in Figs. 5–7.

C. Interplay of interference and Coulomb effects

In Fig. 5(a) we present the offset angles of the PMD predicted by the TDSE, the L-TRCM model, and the L-TRCM model neglecting the interference effect, for 2D H_2^+ with different R at laser intensity $I = 1\times10^{15}$ W/cm^2. When the internuclear distance R changes from 14 to 20 a.u., the offset angles of the TDSE for H_2^+ are located in a small range of 22.6°–23.4°. The predictions of the L-TRCM model for the offset angle at different R are also located in a small range of 20.5°–21.1°. There is a difference of about 1.3°–2.3° between the results of the TDSE and the L-TRCM model. By comparison, the L-TRCM model neglecting the interference effect predicts the angles which are located in the range of 16.7°–17.9°. Specifically, this model assumes $\mathbf{d}_f(\mathbf{v}) = \mathbf{d}_a(\mathbf{v})$ in Eq. (16), which neglects the cos interference term, and uses the expression (22) with the lag τ calculated through Eq. (29) at the peak time t_p. Then Eq. (30) gives the PMD from which the offset angle of the L-TRCM-N model in Fig. 5(a) is obtained. This means that the interference effect increases the offset angle by about 3.6°. The phenomenon is easy to understand. The cos term will change the amplitude of the photoelectron, resulting in a shift of the momentum which has the largest amplitude.

In Fig. 5(b) we show the lag τ evaluated with the expression of $\tau = \varepsilon\theta/\omega$ for these angles of the TDSE and the L-TRCM model in Fig. 5(a) and the τ evaluated with Eq. (29) corresponds to the lag of the L-TRCM-N model [55]. As discussed in [41], for atoms, instead of the response-time formula (23), the expression $\tau = \varepsilon\theta/\omega$ can also be used to approximately deduce the lag (i.e., the response time of electrons within an atom to a laser-induced tunneling ionization event) from the angle measured in experiments. This approximate expression of τ corresponds to the adiabatic version of the TRCM model where the exit velocity $\mathbf{v}(t_0)$ is neglected [41]. Here we compare the adiabatic prediction of this expression for τ with that of Eq. (29). From the results in Fig. 5(b), one can observe that, due to the interference effect, the time lag deduced with the expression $\tau = \varepsilon\theta/\omega$ differs somewhat from that calculated directly by the response-time formula (29) for molecules with large R. However, these lag curves calculated using different methods show a similar trend, that is, when the distance R is large enough, the lag is not sensitive to the distance R. Specifically, the results of the TDSE for different R are around 146 as, those of the L-TRCM model are around 134 as, and the predictions of Eq. (29) are located in a small range of 116–124 as. These results suggest that for cases of large R, one can still use this expression of $\tau = \varepsilon\theta/\omega$ to approximately deduce the lag from the measured angle. We mention that the results of lag for large R in Fig. 5(b) are remarkably larger than 82 as predicted by Eq. (25) for H_2^+ with $R = 2$ a.u., and 65 as predicted by Eq. (23) for the model atom with similar I_p to H_2^+.

In Fig. 5(c) we present the exit position $r_0'' = |x_2 - x_1|$ obtained from the laser-dressed potential [also see Fig. 1(b)] at the corresponding internuclear distance. This exit position is used to determine the parameter r_d in the L-TRCM model to obtain the offset angle of the PMD in Fig. 5(a). The exit positions r_0'' are 4.85 a.u. for the case of $R = 14$ a.u., 5.22 a.u. for $R = 16$ a.u., 5.61 a.u. for $R = 18$ a.u., and 5.64 a.u. for $R = 20$ a.u. The exit position increases slightly with the increase of internuclear distance. This slow increase may be the reason why the curves in Figs. 5(a) and 5(b) change slowly with increasing internuclear distance. It also indicates that for the cases of large R, the influence of another nucleus on the exit position of the dressed-up barrier decreases slightly with the increase of R.

In Fig. 6(a) we present the offset angles of the PMD predicted by the TDSE, the L-TRCM model, and the L-TRCM model neglecting the interference effect, for 2D H_2^+ with $R = 16$ a.u. at different laser intensities. As the laser intensity increases from 0.6×10^{15} W/cm^2 to 1.2×10^{15} W/cm^2, the offset angle predicted by the TDSE increases from 20° to 23.3°. The offset angles predicted by the L-TRCM model are located in a small range of 20.9°–21.3°. There is a difference of about 0.1°–2.1° between the results of the TDSE and the L-TRCM model. The difference between curves of the TDSE and the L-TRCM model in Fig. 6(a) is smaller for lower laser intensities, suggesting that the L-TRCM model seems more applicable for lower laser intensities. These angles predicted by the L-TRCM model neglecting the cos term in Eq. (16) are located in a range of 17.1°–18.2° and are smaller than those predicted by the L-TRCM model. Results in Fig. 6(b) are similar to Fig. 5(b) and show the corresponding time lags for these angles in Fig. 6(a). As the black and red curves of lag in Fig. 6(b) are close at lower laser intensities, but the corresponding black and red curves of the angle in Fig. 6(a) deviate

from each other at lower intensities, one can expect that the relation of $\tau = \varepsilon\theta/\omega$, which is related to the adiabatic version of the TRCM model and is used to obtain the black lag curve in Fig. 6(b) from the black angle curve in Fig. 6(a), works better for higher laser intensities. In Fig. 6(c) we present the exit position r_0'' obtained from the laser-dressed potential at the corresponding laser intensity. In this case, the exit position decreases slightly with the increase of laser intensity. This is easy to understand because for higher laser intensities, the Coulomb potential is more significantly bent by the laser field.

For a comprehensive comparison, in Fig. 7 we present the ratios of $(\theta'' - \theta')/\theta''$ for 2D H_2^+ at different internuclear distances R and varied laser intensities. Here θ'' is the offset angle predicted by the TDSE and θ' is that predicted by the L-TRCM model. The main phenomena shown in Fig. 7 are that (i) for a fixed laser intensity, the ratio curve increases remarkably with the increase of R and becomes insensitive to R for $R \geqslant 17$ a.u., suggesting that for cases with larger R, the influence of another nucleus on the tunnel exit becomes insensitive to the increase of R, and (ii) for a fixed distance R, the ratio is smaller for lower laser intensities on the whole, suggesting that the L-TRCM model works better for lower intensities. In particular, for all cases, the values of ratio are close to or less than 10%, indicating the applicability range of the L-TRCM model. The remaining difference between predictions of the L-TRCM model and the TDSE may arise from the following reasons. Strong-field ionization of H_2^+ with large R involves a complex four-body interaction between the electron, the laser, and these two nuclei. Due to the effect of charge resonance, electrons tend to escape through tunneling out of the dressed-up barrier near one of the two nuclei of the molecule. This barrier is influenced by another nucleus of the molecule, as discussed in Fig. 1(b). In the L-TRCM model, we approximate this influence by simply correcting the tunnel exit. This approximation is not precise enough. Therefore, the predictions of the L-TRCM model may differ somewhat from the results of the TDSE.

We mention that the Coulomb effect can also be considered with the modified SFA (MSFA) model [51], where the Coulomb potential is included in the evolution of the system after tunneling, with the solution of the Newton equation including both the electric-field force and the Coulomb force. For atoms and molecules with small R, the MSFA is able to predict nonzero offset angles which are several degrees smaller than those predicted by the TDSE and the TRCM model [53]. For molecules with large R, however, the situation is different. In the MSFA simulation, electrons tunneling from one nucleus will encounter another nucleus shortly after tunneling. The Coulomb effect of the second nucleus may lead to some unpredictable structures in the PMD, resulting in significant differences between the results of the MSFA and TDSE.

D. Further consideration of 3D cases

The above discussion focuses on 2D cases. To further check the results, we have also performed 3D simulations. Relevant results are presented in Fig. 8, where we plot the PMDs of 3D H_2^+ with different R obtained with the TDSE and the L-TRCM model. For the L-TRCM model in 3D cases, we use the value of $n_f = 3$ in Eq. (29), and the whole effective charges Z' used in Eq. (29) are $Z' = 4.136$ for $R = 16$ a.u., $Z' = 4.17$ for $R = 18$ a.u., and $Z' = 4.202$ for $R = 20$ a.u. For the TDSE results in the left column of Fig. 8, it can be observed that the offset angles of 3D cases are 3.3°–4.9° smaller than the corresponding 2D ones shown in Figs. 2 and 4. The 3D TRCM model results in the right column of Fig. 8 are also in quantitative agreement with the 3D TDSE results, with a difference smaller than 1.7°.

It should be mention that in Ref. [56], the 3D TDSE for H_2^+ was solved and the important influence of large internuclear distances on the photoelectron energy spectrum was revealed. In this case both the ground and excited states should be incorporated in the SFA model. In addition, ionization from the coherent superposition of states and a comparison of the modified SFA with the 3D TDSE were given in Ref. [57]. The DSFA introduced in Sec. II B 2 in this paper is similar to the modified SFA in Ref. [57]. In this modified SFA, the energy difference between these two electronic states is small and nonzero. In the DSFA, these two states are considered to be degenerate.

IV. CONCLUSION

We have studied tunneling ionization of H_2^+ with large R in strong elliptically polarized laser fields, in comparison to model atoms and H_2^+ with small R. Our research indicates that both the strong coupling between the ground state and the first excited state of the system and the two-center Coulomb potential of large R have significant effects on the ionization process of the stretched molecule. The TDSE simulations show that the offset angle in the PMD for cases of large R is remarkably larger than the cases of small R and atoms with similar ionization potentials, and the PMDs for cases of large R show clear interference patterns which disappear for cases of small R. By developing a strong-field model, the L-TRCM model, which considers both the effects of the first excited state and the two-center Coulomb potential of large R, we were able to reproduce the typical results of the TDSE. We showed that the interference patterns are closely related to the effect of charge resonance between these two lowest states of H_2^+ with large R. In particular, the strong-field ionization process for the case of large R involves a strong four-body interaction between the electron, the laser, and these two nuclei of the molecule. The laser-dressed two-center Coulomb potential forms two potential barriers near the two nuclei: one dressed up and another dressed down. The dressed-up barrier near one of the two nuclei is influenced by another nucleus and is lower and narrower than the dressed-down one. Therefore, electrons tend to escape from the dressed-up barrier. This property allowed us to approximate the complex four-body interaction as the three-body one between the electron, the laser, and the nucleus neighboring the dressed-up barrier, taking into consideration the influence of another nucleus on the dressed-up barrier as a correction to the tunnel exit. The L-TRCM model based on the above approximations suggests a simple method for studying time-resolved ionization dynamics of molecules with large R. It also provides a manner for probing the characteristics of Coulomb potential of stretched molecules. In addition, we also discussed the possible response time of the electron to light, referred to as the Coulomb-induced ionization time lag,

in strong-field tunneling ionization of molecules with large R. This time is calculated by a simple expression composed of basic laser and molecular parameters and reflects the time scale of the strong four-body interaction between the laser, the electron, and these two nuclei of the molecule. As the offset angles deduced from the calculated time agree with the TDSE ones, our simulations show that for tunneling ionization of molecules with large R, the response time is larger than that of model molecules with small R, but becomes insensitive to the increase of the distance R when this distance is large enough.

ACKNOWLEDGMENT

This work was supported by the National Natural Science Foundation of China (Grants No. 12174239, No. 12347165, and No. 12404330).

[1] A. McPherson, G. Gibson, H. Jara, U. Johann, T. S. Luk, I. A. McIntyre, K. Boyer, and C. K. Rhodes, Studies of multiphoton production of vacuum-ultraviolet radiation in the rare gases, J. Opt. Soc. Am. B **4**, 595 (1987).

[2] A. L'Huillier, K. J. Schafer, and K. C. Kulander, Theoretical aspects of intense field harmonic generation, J. Phys. B **24**, 3315 (1991).

[3] P. B. Corkum and F. Krausz, Attosecond science, Nat. Phys. **3**, 381 (2007).

[4] F. Krausz and M. Ivanov, Attosecond physics, Rev. Mod. Phys. **81**, 163 (2009).

[5] F. Lépine, M. Y. Ivanov, and M. J. J. Vrakking, Attosecond molecular dynamics: Fact or fiction, Nat. Photon. **8**, 195 (2014).

[6] Z. Tao, C. Chen, T. Szilvási, M. Keller, M. Mavrikakis, H. Kapteyn, and M. Murnane, Direct time-domain observation of attosecond final-state lifetimes in photoemission from solids, Science **353**, 62 (2016).

[7] P. B. Corkum, Plasma perspective on strong field multiphoton ionization, Phys. Rev. Lett. **71**, 1994 (1993).

[8] M. Lewenstein, P. Balcou, M. Y. Ivanov, A. L'Huillier, and P. B. Corkum, Theory of high-harmonic generation by low-frequency laser fields, Phys. Rev. A **49**, 2117 (1994).

[9] C. M. Heyl, P. Rudawski, F. Brizuela, S. N. Bengtsson, J. Mauritsson, and A. L'Huillier, Macroscopic effects in non-collinear high-order harmonic generation, Phys. Rev. Lett. **112**, 143902 (2014).

[10] P. Stammer, J. Rivera-Dean, A. S. Maxwell, T. Lamprou, J. Argüello-Luengo, P. Tzallas, M. F. Ciappina, and M. Lewenstein, Entanglement and squeezing of the optical field modes in high harmonic generation, Phys. Rev. Lett. **132**, 143603 (2024).

[11] S. Qiao, L. Li, P. Lan, and P. Lu, Electron-wave-packet-deformation-induced attosecond emission time shift in gas high-order harmonic generation, Phys. Rev. A **109**, 023121 (2024).

[12] F. Yergeau, G. Petite, and P. Agostini, Above-threshold ionization without space charge, J. Phys. B **19**, L663 (1986).

[13] R. R. Freeman, T. J. McIlrath, P. H. Bucksbaum, and M. Bashkansky, Ponderomotive effects on angular distributions of photoelectrons, Phys. Rev. Lett. **57**, 3156 (1986).

[14] G. G. Paulus, W. Nicklich, H. Xu, P. Lambropoulos, and H. Walther, Plateau in above threshold ionization spectra, Phys. Rev. Lett. **72**, 2851 (1994).

[15] A. Lohr, M. Kleber, R. Kopold, and W. Becker, Above-threshold ionization in the tunneling regime, Phys. Rev. A **55**, R4003 (1997).

[16] S. Beaulieu, A. Comby, A. Clergerie, J. Caillat, D. Descamps, N. Dudovich, B. Fabre, R. Géneaux, F. Légaré, S. Petit, B. Pons, G. Porat, T. Ruchon, R. Taïeb, V. Blanchet, and Y. Mairesse, Attosecond-resolved photoionization of chiral molecules, Science **358**, 1288 (2017).

[17] J. Yuan, Y. Ma, R. Li, H. Ma, Y. Zhang, D. Ye, Z. Shen, T. Yan, X. Wang, M. Weidemüller, and Y. Jiang, Momentum spectroscopy for multiple ionization of cold rubidium in the elliptically polarized laser field, Chin. Phys. Lett. **37**, 053201 (2020).

[18] K. Lin, S. Brennecke, H. Ni, X. Chen, A. Hartung, D. Trabert, K. Fehre, J. Rist, X.-M. Tong, J. Burgdörfer, L. P. H. Schmidt, M. S. Schöffler, T. Jahnke, M. Kunitski, F. He, M. Lein, S. Eckart, and R. Dörner, Magnetic-field effect in high-order above-threshold ionization, Phys. Rev. Lett. **128**, 023201 (2022).

[19] T. Shaaran, M. T. Nygren, and C. F. Faria, Laser-induced nonsequential double ionization at and above the recollision-excitation-tunneling threshold, Phys. Rev. A **81**, 063413 (2010).

[20] W. Becker, X. J. Liu, P. J. Ho, and J. H. Eberly, Theories of photoelectron correlation in laser-driven multiple atomic ionization, Rev. Mod. Phys. **84**, 1011 (2012).

[21] F. Li, Y.-J. Yang, J. Chen, X.-J. Liu, Z.-Y. Wei, and B.-B. Wang, Universality of the dynamic characteristic relationship of electron correlation in the two-photon double ionization process of a helium-like system, Chin. Phys. Lett. **37**, 113201 (2020).

[22] P. Eckle, M. Smolarski, P. Schlup, J. Biegert, A. Staudte, M. Schöffler, H. G. Muller, R. Dörner, and U. Keller, Attosecond angular streaking, Nat. Phys. **4**, 565 (2008).

[23] C. I. Blaga, F. Catoire, P. Colosimo, G. G. Paulus, H. G. Muller, P. Agostini, and L. F. DiMauro, Strong-field photoionization revisited, Nat. Phys. **5**, 335 (2009).

[24] M. Paul, L. Yue, and S. Gräfe, Imprints of the molecular electronic structure in the photoelectron spectra of strong-field ionized asymmetric triatomic model molecules, Phys. Rev. Lett. **120**, 233202 (2018).

[25] W. Becker, F. Grasbon, R. Kopold, D. B. Milošević, G. G. Paulus, and H. Walther, Above-threshold ionization: From classical features to quantum effects, Adv. At. Mol. Opt. Phys. **48**, 35 (2002).

[26] P. Eckle, A. N. Pfeiffer, C. Cirelli, A. Staudte, R. Dörner, H. G. Muller, M. Buttiker, and U. Keller, Attosecond ionization and tunneling delay time measurements in helium, Science **322**, 1525 (2008).

[27] A. N. Pfeiffer, C. Cirelli, M. Smolarski, D. Dimitrovski, M. Abu-samha, L. B. Madsen, and U. Keller, Attoclock reveals natural coordinates of the laser-induced tunnelling current flow in atoms, Nat. Phys. **8**, 76 (2012).

[28] A. S. Landsman, M. Weger, J. Maurer, R. Boge, A. Ludwig, S. Heuser, C. Cirelli, L. Gallmann, and U. Keller, Ultrafast resolution of tunneling delay time, Optica **1**, 343 (2014).

[29] N. Camus, E. Yakaboylu, L. Fechner, M. Klaiber, M. Laux, Y. Mi, K. Z. Hatsagortsyan, T. Pfeifer, C. H. Keitel, and R. Moshammer, Experimental evidence for quantum tunneling time, Phys. Rev. Lett. **119**, 023201 (2017).

[30] U. S. Sainadh, H. Xu, X. Wang, A. Atia-Tul-Noor, W. C. Wallace, N. Douguet, A. W. Bray, I. Ivanov, K. Bartschat, A. Kheifets, R. T. Sang, and I. V. Litvinyuk, Attosecond angular streaking and tunnelling time in atomic hydrogen, Nature (London) **568**, 75 (2019).

[31] W. Quan, V. V. Serov, M. Wei, M. Zhao, Y. Zhou, Y. Wang, X. Lai, A. S. Kheifets, and X. Liu, Attosecond molecular angular streaking with all-ionic fragments detection, Phys. Rev. Lett. **123**, 223204 (2019).

[32] J. Chen and S. G. Chen, Gauge problem in molecular high-order harmonic generation, Phys. Rev. A **75**, 041402(R) (2007).

[33] W. Becker, J. Chen, S. G. Chen, and D. B. Milošević, Dressed-state strong-field approximation for laser-induced molecular ionization, Phys. Rev. A **76**, 033403 (2007).

[34] Y. J. Chen and B. Zhang, Strong-field approximations for the orientation dependence of the total ionization of homonuclear diatomic molecules with different internuclear distances, J. Phys. B **45**, 215601 (2012).

[35] S. Wang, J. Cai, and Y. J. Chen, Ionization dynamics of polar molecules in strong elliptical laser fields, Phys. Rev. A **96**, 043413 (2017).

[36] M. Lewenstein, K. C. Kulander, K. J. Schafer, and P. H. Bucksbaum, Rings in above-threshold ionization: A quasiclassical analysis, Phys. Rev. A **51**, 1495 (1995).

[37] W. Y. Li, S. Wang, Y. Z. Shi, S. P. Yang, and Y. J. Chen, Probing the structure of stretched molecular ions with high-harmonic spectroscopy, J. Phys. B **50**, 085003 (2017).

[38] T. Zuo and A. D. Bandrauk, Charge-resonance-enhanced ionization of diatomic molecular ions by intense lasers, Phys. Rev. A **52**, R2511 (1995).

[39] S. P. Goreslavski, G. G. Paulus, S. V. Popruzhenko, and N. I. Shvetsov-Shilovski, Coulomb asymmetry in above-threshold ionization, Phys. Rev. Lett. **93**, 233002 (2004).

[40] M. D. Feit, J. A. Fleck, and A. Steiger, Solution of the Schrödinger equation by a spectral method, J. Comput. Phys. **47**, 412 (1982).

[41] J. Y. Che, C. Chen, W. Y. Li, S. Wang, X. J. Xie, J. Y. Huang, Y. G. Peng, G. G. Xin, and Y. J. Chen, Response time of photoemission at quantum-classic boundary, arXiv:2111.08491.

[42] J. Y. Che, F. B. Zhang, W. Y. Li, C. Chen, and Y. J. Chen, Single-photon ionization of aligned H_2^+ with near-ionization-threshold photon energy, New J. Phys. **25**, 083022 (2023).

[43] Y. J. Chen and B. Hu, Intense field ionization of diatomic molecules: Two-center interference and tunneling, Phys. Rev. A **81**, 013411 (2010).

[44] F. J. Sun, C. Chen, W. Y. Li, X. Liu, W. Li, and Y. J. Chen, High ellipticity of harmonics from molecules in strong laser fields of small ellipticity, Phys. Rev. A **103**, 053108 (2021).

[45] D. Ren, S. Wang, C. Chen, X. Li, X. Yu, X. Zhao, P. Ma, C. Wang, S. Luo, Y. Chen, and D. Ding, Alignment dependence of photoelectron momentum distributions for diatomic molecule N_2 in strong elliptical laser fields, J. Phys. B **55**, 175101 (2022).

[46] Y. Chen, J. Chen, and J. Liu, Charge-resonance effect on harmonic generation by symmetric diatomic molecular ions in intense laser fields, Phys. Rev. A **74**, 063405 (2006).

[47] W. Li, F. Dong, S. Yu, S. Wang, S. Yang, and Y. Chen, Ellipticity of near-threshold harmonics from stretched molecules, Opt. Express **23**, 31010 (2015).

[48] B. Yang, K. J. Schafer, B. Walker, K. C. Kulander, P. Agostini, and L. F. DiMauro, Intensity-dependent scattering rings in high order above-threshold ionization, Phys. Rev. Lett. **71**, 3770 (1993).

[49] T. Brabec, M. Y. Ivanov, and P. B. Corkum, Coulomb focusing in intense field atomic processes, Phys. Rev. A **54**, R2551 (1996).

[50] T. M. Yan, S. V. Popruzhenko, M. J. J. Vrakking, and D. Bauer, Low-energy structures in strong field ionization revealed by quantum orbits, Phys. Rev. Lett. **105**, 253002 (2010).

[51] X. Xie, C. Chen, G. Xin, J. Liu, and Y. Chen, Coulomb-induced ionization time lag after electrons tunnel out of a barrier, Opt. Express **28**, 33228 (2020).

[52] S. Wang, J. Y. Che, C. Chen, G. G. Xin, and Y. J. Chen, Tracing origins of asymmetric momentum distribution for polar molecules in strong linearly polarized laser fields, Phys. Rev. A **102**, 053103 (2020).

[53] Y. G. Peng, J. Y. Che, F. B. Zhang, X. J. Xie, G. G. Xin, and Y. J. Chen, Response time of an electron inside a molecule to light in strong-field ionization, Opt. Express **32**, 12734 (2024).

[54] Z. Y. Chen *et al.*, Coulomb-related symmetry in laser-induced tunneling ionization of atoms and molecules (unpublished).

[55] J. Y. Che, J. Y. Huang, F. B. Zhang, C. Chen, G. G. Xin, and Y. J. Chen, Roles of laser ellipticity in attoclocks, Phys. Rev. A **107**, 043109 (2023).

[56] B. Fetić and D. B. Milošević, High-order above-threshold ionization of the H_2^+ ion: The role of internuclear distance, Phys. Rev. A **99**, 043426 (2019).

[57] D. B. Milošević, B. Fetić, and P. Ranitovic, High-order above-threshold ionization from a coherent superposition of states, Phys. Rev. A **106**, 013109 (2022).